Structural Modeling of the Distamycin A–d(CGCGAATTCGCG)$_2$ Complex Using 2D NMR and Molecular Mechanics†

Jeffrey G. Pelton and David E. Wemmer*

Department of Chemistry, University of California, and Chemical Biodynamics Division, Lawrence Berkeley Laboratory, 1 Cyclotron Road, Berkeley, California 94720

Received December 28, 1987; Revised Manuscript Received May 27, 1988

ABSTRACT: The structure of the distamycin A–d(CGCGAATTCGCG)$_2$ complex has been determined through a combination of SKEWSY and NOESY 2D NMR experiments and molecular mechanics calculations. NMR data provided upper bounds on many proton–proton pairs. The advantage of the SKEWSY/NOESY method is that small groups of strongly coupled spins can be treated accurately as isolated systems. The AMBER molecular mechanics package, modified to include the NMR constraints, was used in energy refinements. Distamycin A fits snugly into the 5′-AATT-3′ minor-groove binding site. Structural analysis revealed van der Waals contacts between A5, A6, and A18 C2H and drug H3 protons, potential three-center hydrogen bonding between drug amide protons and adenine N3 and thymine O2 atoms analogous to the spine of hydration in the crystal structure of the free DNA, and stacking of the sugar O1′ atoms of A6–C21, T7–T20, and, T8–T19, over drug pyrrole rings 1, 2, and 3, respectively. In addition to hydrophobic effects, hydrogen bonding, and electrostatic interactions proposed by others, it is suggested that stacking interactions between DNA sugar O1′ atoms and the three drug pyrrole rings contribute to the stability of the complex.

Understanding the structure, sequence specificity, and forces responsible for the binding of antibiotics to DNA molecules is an important first step in the design of new drugs and sequence-specific probes. Distamycin A (Figure 1) and netropsin (two *N*-methylpyrrolecarboxamide units and a guanidinoacetyl group in place of the formamide group of distamycin A) are examples of nonintercalating antibiotics that bind preferentially to the minor groove of A-T- and I-C-rich B-form DNA sequences (Krey et al., 1973) [for reviews see Hahn (1975) and Zimmer (1975)]. Footprinting and affinity cleaving studies have shown that distamycin A binds preferentially to 5′-AAATT-3′, in both orientations to a degree dependent on flanking sequences (Taylor et al., 1984; Dervan, 1986). Zimmer et al. (1972) have shown that increasing the number of *N*-methylpyrrolecarboxamide units of distamycin A from three to four and five increases the stability of the drug–DNA complex. He attributed the increased stability to hydrophobic effects associated with the drug pyrrole rings. NMR studies of netropsin with d(CGCGAATTCGCG)$_2$ established that DNA adenine C2H and drug H3 protons were in van der Waals contact (Patel, 1982), while later NMR studies of netropsin with d(GGAATTCC)$_2$ revealed intermolecular contacts between netropsin amide and CH protons and DNA adenine C2H and sugar H1′ protons (Patel & Shapiro, 1985). These contacts were also observed in the crystal structure of netropsin with d(CGCGAATTCGCG)$_2$ (Kopka et al., 1985a–c). A recent crystal structure of the distamycin A–d(CGCAAATTTGCG)$_2$ complex (Coll et al., 1987) has confirmed many of the same features about binding of these *N*-methylpyrrolecarboxamide-containing drugs. On the basis of available data, some believe that hydrogen bonds and electrostatic forces are responsible for the strong binding of netropsin and distamycin A and that van der Waals contacts between adenine C2H and drug CH protons determine the sequence specificity (Kopka et al., 1985c). Others believe electrostatic forces are the main determinant of specificity (Zakrzewska et al., 1987; Lavery et al., 1986).

Recently, the NMR resonance assignments, the kinetics, and a qualitative structure of the distamycin A–d(CGCGAATTCGCG)$_2$ complex were reported (Klevit et al., 1986). We have quantified the structure of this complex by further application of 2D NMR[1] techniques and molecular mechanics calculations. It is hoped that this and similar NMR studies will provide a molecular basis for the interaction of distamycin A with various DNA sequences. In addition, NMR should play an important role both in identifying multiple binding sites and in determining the major and minor orientations of the drug at these sites on longer A-T sequences.

To obtain as accurate constraints as possible for our modeling studies, we began quantitative interpretation of NOESY spectra (Jeener et al., 1979). However, these spectra were complicated by the fact that both relatively short and long drug–DNA contacts occur. Extension of the mixing time to increase the intensities of the long-distance contacts resulted in significant spin diffusion in the short-range contacts. Spin diffusion was included in the analysis by using both SKEWSY (Bremer et al., 1984) and NOESY experiments, which taken together provided upper bounds for many DNA–DNA and drug–DNA proton distances. These constraints were added to a modified AMBER (Weiner et al., 1984) molecular mechanics potential function to generate a structure of the complex. Structural analysis revealed that, in addition to van der Waals contacts between drug CH and adenine C2H protons and potential three-center drug–DNA hydrogen bonds, that DNA O1′ atoms that lie along the walls of the minor groove sandwich each of the three pyrrole rings of the drug. These

† This work was supported by NIH through the L.B.L. BRSG program and equipment grants from the DOE University Research Instrumentation program (DE F605 86ER75281) and NSF (DMB 8609035).

[1] Abbreviations: 2D NMR, two-dimensional nuclear magnetic resonance; NOE, nuclear Overhauser effect; 1D NOE, one-dimensional nuclear Overhauser effect; NOESY, two-dimensional NOE spectroscopy; SKEWSY, skewed exchange spectroscopy; AMBER, assisted model building and energy refinement.

0006-2960/88/0427-8088$01.50/0

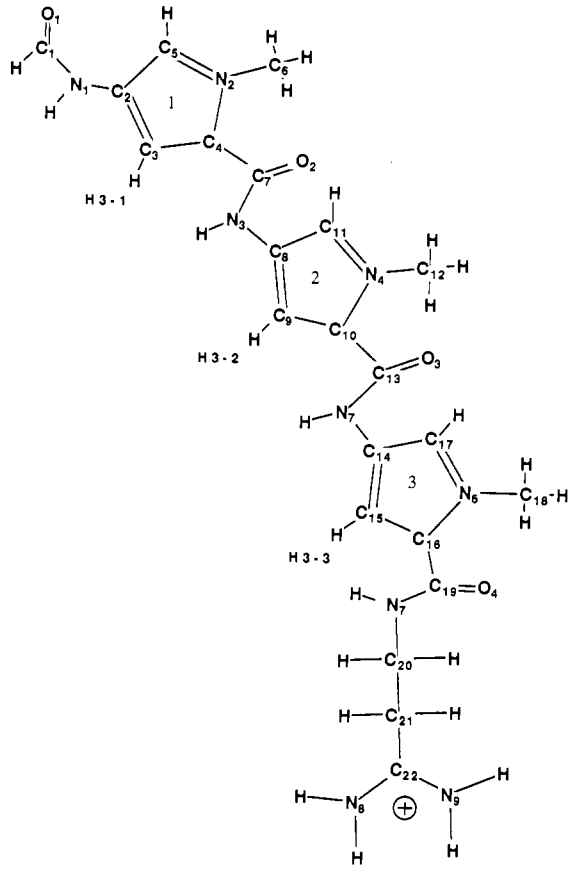

FIGURE 1: Structure and numbering scheme for distamycin A. The drug consists of a formamide unit, three *N*-methylpyrrolecarboxamide units, and a positively charged propylamidinium unit.

stacking interactions may contribute to the stability of the complex.

Materials and Methods

NMR Spectroscopy. NMR samples were prepared as described previously (Klevit et al., 1986). NMR spectra were obtained on a GN-500 spectrometer. SKEWSY and NOESY experiments were obtained in phase-sensitive mode using TPPI (Drobny et al., 1979). NOESY experiments were obtained at 50-, 100-, 150-, 200-, 250-, and 500-ms mixing times. A SKEWSY experiment was obtained in which both delay periods were 500-ms. This value was chosen to ensure that sufficient relaxation occurred during t_s to differentiate the SKEWSY and NOESY peak volumes. All experiments were conducted at 13.5 °C to limit chemical exchange of the drug between equivalent sites on the DNA (Klevit et al., 1986). For each t_1 64 scans were signal averaged, taking 1024 complex points with a recycle time of 2.1 s; 512 t_1s were recorded per experiment. An additional NOESY experiment was obtained with a mixing time of 100 ms and a recycle delay of 10.2 s. A spectral width of 5000 Hz resulted in a digital resolution of 4.9 Hz/point. The residual HDO resonance was saturated during both the recycle and mixing times. The data were transferred to tape and processed with FTNMR software (Hare Research) on Vaxstation II or Vax 11/785 computers. In t_2 the data were apodized with a sine-bell window function phase shifted 60° and skewed toward the beginning of the FID prior to Fourier transformation. In t_1 the data were zero filled to 2048 complex points and apodized as in t_2 prior to the second Fourier transformation. Peak volumes were measured by using FTNMR. Background peak volumes defined in regions with no signal were subtracted before calculations were performed.

Table I: Atom Types and Point Charges for Distamycin A

atom	atom type	point charge	atom	atom type	point charge
O1	C	−0.20	N4	NA	−0.21
C1	C	0.35	C12	CT	0.22
HF	HC	0.03	C12H	HC	0.01
N1	N	−0.32	C10	CW	−0.07
HN1/3/5	H	0.18	C14	CM	0.03
C2	CM	−0.15	C17	CW	0.02
C3	CM	−0.07	H17	HC	0.14
H3/9/15	HC	0.09	N6	NA	−0.20
C5	CW	−0.01	C18	CT	0.19
H5	HC	0.12	C18H	HC	0.01
N2	NA	−0.17	C16	CW	−0.12
C6	CT	0.21	C19	C	0.43
C6H	HC	0.01	O4	O	−0.31
C4	CW	−0.13	N7	N	−0.40
C7/13	C	0.44	HN7	H	0.17
O2/3	O	−0.37	C20	CT	0.17
N3/N5	N	−0.34	C20H	HC	0.02
C8	CM	0.00	C21	CT	−0.04
C9/15	CM	−0.08	C21H	HC	0.07
C11	CW	0.02	C22	CA	0.39
H11	HC	0.11	N8/9	N2	−0.28
NH8/9	H3	0.25			

Molecular Mechanics Calculations. The initial DNA coordinates were taken from the crystal structure of d-(CGCGAATTCGCG)$_2$ (Fratini et al., 1982). The initial distamycin A structure was created by using the crystal structure of netropsin (Berman et al., 1979) and standard angles and distances. Protons were added with inhouse software. Energy refinements were performed with a modified version of the AMBER molecular mechanics package. NMR constraints were included by adding the following term to the normal potential function:

$$E_{NMR} = K_{NMR}(R - R_0)^2 \quad \text{if } R \geq R_0$$

$$E_{NMR} = 0.0 \quad \text{if } R < R_0$$

R_0 is the upper bound on a given proton–proton distance, and K_{NMR} is an adjustable force constant. Point charges for distamycin A were determined from MNDO (Dewar & Theil, 1977) calculations. Atom types and point charges used for the distamycin A refinement are presented in Table I. All-atom force field parameters for the nucleic acid were taken from those described previously (Weiner et al., 1986). Most distamycin A force field parameters were taken from the united atom model of netropsin (Caldwell & Kollman, 1986) except that Lennard-Jones parameters for the carbon atoms were taken from the all-atom model (Weiner et al., 1986). An angle potential for CW–CM–HC (AMBER atom types) of 35.0 (kcal/mol)/deg^2 and 109.5° and specific torsional parameters for C–CW–CM–HC of 6.59 kcal/mol and 180° and for HC–CW–NA–CT of 1.71 kcal/mol and 180° were added to the standard database. These parameters were estimated from values reported for CM–CM–HC, C–CM–CM–HC, and HC–CM–CM–CT, respectively (Weiner et al., 1986). All degrees of freedom were refined. A 12-Å nonbonded and 4-Å hydrogen bond cutoff were employed. Solvent effects were accounted for through the use of a distance-dependent dielectric of the form $\epsilon = R$.

Distamycin A and the DNA were separately refined to an rms energy gradient of 0.1 (kcal/mol)/Å. The energy-refined drug was then interactively docked into the minor groove of the DNA by using a PS300 Evans and Sutherland graphics terminal. The adenine C2H to drug H3 contacts indicated by NOESY experiments were used as a guide in the docking procedure. The initial complex was refined with an NMR

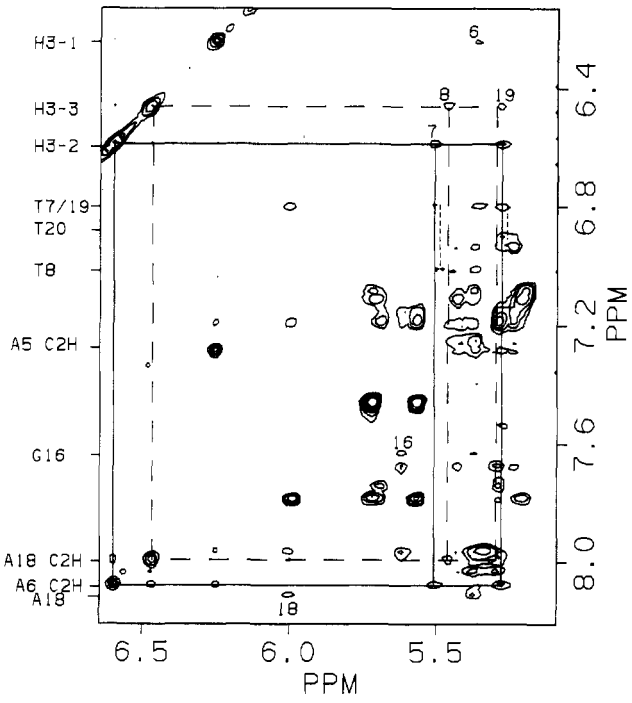

FIGURE 2: NOESY spectrum of the distamycin A–DNA complex. Aromatic to C1′H region of a symmetrized NOESY spectrum taken at 13.5 °C with a mixing time of 500 ms. Aromatic C6H resonances of cytosine and thymine. C8H resonances of adenine and guanine, and C2H resonances of adenine (shown explicitly) are along the vertical axis. Numbers denote the positions of the C1′H resonances along the horizontal axis. T7 and T19 C1′H assignments are reversed with respect to those reported previously (Klevit et al., 1986). Short dashed lines show sequential connectivities between T7 C1′H and T8 C6H and between T19 C1′H and T20 C6H. Solid lines connect resonances A6 C2H, H3-2, T7 C1′H, and T19 C1′H, which comprise one spin system. Long dashed lines connect resonances A18 C2H, H3-3, T8 C1′H, and T19 C1′H, which comprise a second spin system.

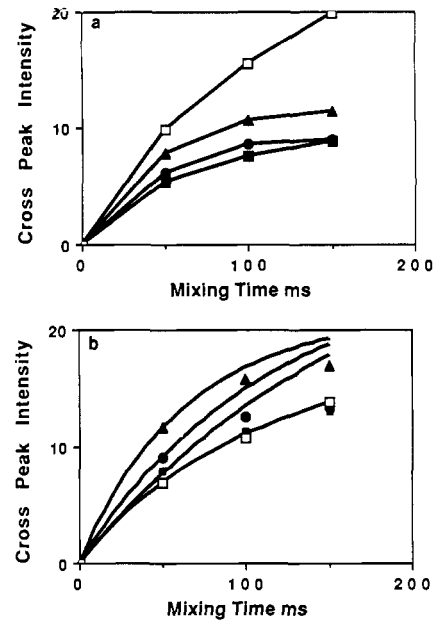

FIGURE 3: Experimental and simulated NOE buildup curves. Experimental points are denoted (□) C11 H5-H6, (▲) H3-3–A18 C2H, (●) H3-2–A6 C2H, and (■) H3-1–A5 C2H. (a) Experimental NOE buildup curves for the distamycin A–DNA complex. Data were taken from NOESY experiments with mixing times of 50, 100, and 150 ms. (b) Simulated NOE buildup curves for the distamycin A–DNA complex. Simulated data are represented by solid lines. DNA adenine C2H–drug H3 buildup curves were simulated by using a four-spin approximation with distances within 0.5 Å of structure H_D (see text). C11 C5H–C6H data were simulated by using a four-spin approximation including C5H, C6H, and CH2′ protons of the same residue and the CH2″ proton of the 5′ neighbor. Distances were taken from idealized B-form coordinates. A correlation time of 6 ns and a spectrometer frequency of 500 MHz were used in all simulations. Adenine C2H–drug H3 experimental points were scaled by 2.1 relative to the C11 data (see text).

force constant, K_{NMR}, of 10000 (kcal/mol)/Å^2 to an rms energy gradient of 0.1 (kcal/mol)/Å. Two structures were then further refined by employing NMR force constants of 10000 and 0.59 (kcal/mol)/Å^2 to an rms energy gradient of 0.05 (kcal/mol)/Å. The dependence of the final AMBER structure on starting coordinates was investigated by refining a complex derived from idealized B-form coordinates (Arnott and Chandrasekaran, private communication) using an NMR force constant of 10000 (kcal/mol)/Å^2 to an rms energy gradient of 0.05 (kcal/mol)/Å.

Buildup Curves. Buildup curves were calculated by numerical integration of the following differential equations (Kalk & Berendsen, 1976):

$$\frac{dM_i}{dt} = -\rho_i M_i - \sum_{j \neq i} \sigma_{ij} M_j$$

$$\rho_i = \frac{\hbar^2\gamma^4}{10} \sum_{j \neq i} \frac{1}{r_{ij}^6} \left[\tau_c + \frac{3\tau_c}{1 + (\omega\tau_c)^2} + \frac{6\tau_c}{1 + 4(\omega\tau_c)^2} \right] \quad (1)$$

$$\sigma_{ij} = \frac{\hbar^2\gamma^4}{10} \frac{1}{r_{ij}^6} \left[\frac{6\tau_c}{1 + 4(\omega\tau_c)^2} - \tau_c \right]$$

Isotropic rotation and one correlation time for all proton pairs were assumed.

Structural Analysis. NOESY Experiments. Klevit et al. (1986) reported several abnormalities in the NOESY spectrum of the complex at 27 °C. Specifically, the C8H to C1′H resonances of residues G16[2] and A18 were missing from the sequential connectivity pattern of strand 2. These peaks appear in our spectra (Figure 2) taken at 13.5 °C, indicating these residues do not undergo large structural changes.

Our data also suggest that the previously reported (Klevit et al., 1986) C1′H assignments of T7 and T19 should be reversed. The degeneracy of the T7 and T19 C6H resonances along with the complexity of the NOESY spectrum and weak cross-peak intensities make it difficult to assign these C1′H protons to their respective bases by using the sequential connectivity patterns. There were no cross-peaks between the originally assigned T19 C1′H and T20 C6H in NOESY spectra taken at 200, 250, and 500 ms. There were also no cross-peaks between T7 C1′H and T8 C6H at 200 and 250 ms and only a weak cross-peak between these resonances at 500 ms. In contrast, all of these spectra contain cross-peaks from the originally assigned T7 C1′H and T20 C6H. They also contain cross-peaks between T19 C1′H and T8 C6H, although at 500 ms this peak is weak. Therefore, we believe that T7 C1′H should be assigned to 5.60 ppm and T19 C1′H should be assigned to 5.37 ppm. This change does not alter the assigned binding orientation of the drug or the other assignments but would introduce errors during quantitative refinement.

To obtain as accurate constraints as possible for our subsequent molecular mechanics calculations, we attempted to analyze NOESY spectra quantitatively. For a simple two-spin system, in the short mixing time limit (linear regime), the rate

[2] The numbering scheme for the DNA duplex is for the asymmetric dodecamer, i.e., strand 1, residues 1–12, and strand 2, residues 13–24.

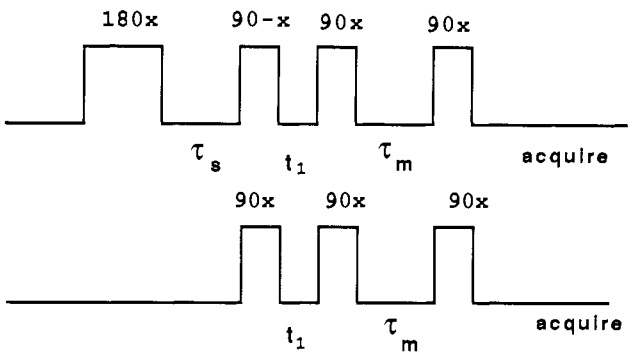

FIGURE 4: SKEWSY and NOESY NMR pulse sequences. The SKEWSY delay periods τ_s and τ_m have the same value as the NOESY mixing time τ_m.

of magnetization transfer is proportional to the inverse sixth power of the distance between the spins. To observe the long-distance NOEs the NOESY mixing time was increased. However, this resulted in spin diffusion for the short-range contacts, which severely complicated the analysis. Experimental buildup curves between cytosine C5H and C6H protons and adenine C2H and drug H3 protons are presented in Figure 3a. The approximately linear rate of buildup of the cytosine protons suggest they comprise a two-spin system at short mixing times. However, the nonlinear rate of buildup of the drug to DNA resonances requires a more careful analysis. Klevit et al. (1986) reported cross-peaks in the NOESY spectrum between A6 C2H and both T7 and T19 C1′H and between A18 C2H and both T8 and T19 C1′H (with corrected assignments as discussed above). From the NOESY spectrum presented in Figure 2, these peaks can be seen to be components of two coupled four-spin systems between A6 C2H, H3-2, T7 C1′H, and T19 C1′H and between A18 C2H, H3-3, T8 C1′H, and T19 C1′H. Thus, a normal analysis cannot be used to determine distances between these protons.

Quantitative Distance Measurements. SKEWSY Experiments. The NOESY spectrum, or intensity matrix **a**, can be related to the relaxation matrix **R**, whose off-diagonal elements are proportional to the inverse sixth power of the distance between two spins, by the equation (Macura & Ernst, 1980)

$$\mathbf{a} \propto e^{-\mathbf{R}t_m} \qquad (2)$$

where t_m is the NOESY mixing time. In theory, one NOESY experiment or intensity matrix **a** contains sufficient information to calculate **R**. By taking ratios of cross-relaxation rates (off-diagonal elements of **R**) and provided that the distance between one pair of protons is known (distance marker), the distance between the other pairs can be calculated even in the presence of spin diffusion. In practice, however, **a** cannot usually be determined due to poor resolution of diagonal peaks. To circumvent this problem, Bremer et al. (1984) introduced the SKEWSY experiment. It contains an initial 180° pulse and delay period t_s prior to the normal NOESY sequence (Figure 4). As described by Bremer et al., this sequence transfers diagonal peak information into the cross-peaks. Thus, SKEWSY and NOESY cross-peaks together contain sufficient information to calculate **a** and by back calculation, **R**, and the distances of interest.

The advantage of the SKEWSY/NOESY method is that small sets of spins that are involved in spin diffusion can be treated as isolated systems. Spins that are coupled to these sets of spins, but that are not part of spin diffusion pathways in the set, do not affect the calculation of cross-relaxation rates and hence distances. For example, consider the spin system presented in Figure 5. Spin 1 is coupled to both spins 2 and 3, but spins 2 and 3 are spatially distant and weakly coupled. Buildup curves were used to determine the intensity matrices for both the isolated two-spin (1 and 2) and three-spin systems (data taken at 500 ms). The relaxation matrix **R** for the two-spin system was then calculated directly from the two-spin intensities, and an approximate two-spin relaxation matrix was calculated for the three-spin system by using intensities from only spins 1 and 2. The results are presented in Table II. Comparison of the relaxation matrices reveals that the diagonal element of spin 1 has increased in the approximate case, reflecting an apparent increase in spin–lattice relaxation but that the cross-relaxation rate between spins 1 and 2 (underlined), which contains the distance information, has not been affected. Thus, for determining the distance between spins 1 and 2, introduction of the third spin into the calculations is unnecessary. Its presence is manifested only in a greater rate of spin–lattice relaxation of spin 1.

To simplify the analysis, A6 C2H, H3-2, T7 C1′H, and T19 C1′H and A18 C2H, H3-3, T8 C1′H, and T19 C1′H were treated as separate four-spin groups. The interaction of any member of the set with other protons was neglected for the reasons discussed above. The cross-peak intensities among members of each set along with the drug diagonal peaks of H3-2 and H3-3 were measured from the NOESY (Figure 2) and SKEWSY (not shown) spectra taken with a mixing time of 500 ms. These data were used in the procedure developed by Bremer et al. (1984) to calculate an intensity matrix **a** and from it the relaxation matrix **R**. The results are presented in Table III. Notice that the cross-peak intensities between T7 C1′H and T19 C1′H and between T8 C1′H and T19 C1′H were set to zero. NOESY spectra taken at 200 and 250 ms show no cross-peaks between either of these proton pairs. At 500 ms, however, a weak signal occurs between T7 C1′H and

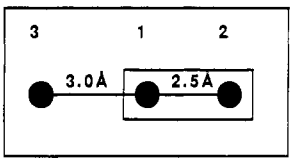

FIGURE 5: Model three-spin system. Model spin system used to determine the effect of spin 3 on the distance calculation between spins 1 and 2.

Table II: Intensity and Relaxation Matrices for the Two- and Three-Spin Systems of Figure 5

	intensity matrix **a**			relaxation matrix **R**	
		Two-Spin System			
(1)		0.32	0.17	2.6	−1.2
(2)		0.17	0.32	<u>−1.2</u>	2.6
		Three-Spin System			
(1)	0.27	0.15	0.06	3.0	−1.2
(2)	0.15	0.32	0.02	<u>−1.2</u>	2.6
(3)	0.06	0.02	0.41		

Table III: Intensity and Relaxation Matrices for the A6 and A18 Spin Systems

	intensity matrix **a**				relaxation matrix **R**			
A6 C2H	0.36	0.26	0.15	0.09	2.9	−1.9	−0.65	−0.32
H3-2	0.26	0.34	0.08	0.08	−1.9	3.0	−0.16	−0.27
T19 C1′H	0.15	0.08	0.55	0.00	−0.65	−0.16	1.29	0.06
T7 C1′H	0.09	0.08	0.00	0.62	−0.32	−0.27	0.06	0.99
A18 C2H	0.15	0.37	0.21	0.14	2.8	−1.3	−0.77	−0.46
H3-3	0.37	0.38	0.12	0.07	−1.3	2.0	−0.48	−0.21
T19 C1′H	0.21	0.12	0.46	0.00	−0.77	−0.48	1.7	0.09
T8 C1′H	0.14	0.07	0.00	0.69	−0.46	−0.21	0.09	0.78

T19 C1′H. This peak is probably due to exchange between the two possible binding orientations of the drug rather than NOE. Since the intensity matrix elements of these spin pairs were set to zero, the relaxation rates 0.06 and 0.09 s^{-1} for T7–T19 and T8–T19, respectively, reflect the experimental uncertainty in the data.

The magnitude of the off-diagonal elements of **R** for both H3-2–A6 C2H and H3-3–A18 C2H reveals that these pairs are strongly coupled and hence spatially close. It can also be seen that T19 C1′H is more strongly coupled to A6 C2H than T7 C1′H and that the T7 sugar is more strongly coupled to the drug H3-2 proton. In addition, T19 C1′H is more strongly coupled to both A18 C2H and H3-3 than is T8 C1′H.

Conversion of cross-relaxation rates to distances still requires a known distance reference, such as that between cytosine C5H and C6H (2.45 Å) (Patel et al., 1987). However, at a 500-ms mixing time, the two-spin approximation is not valid due to spin diffusion from these protons to the CH2′ and CH2″ protons. This could not be corrected by the SKEWSY/NOESY method due to insufficient resolution. However, application of the two-spin approximation to the 50-ms NOESY data (represented by the buildup curve, Figure 3a) does allow for the calculation of upper bounds on the C5H–C6H and A C2H–H3 distances. The upper bounds for A6 C2H–H3-2 and A18 C2H–H3-3 were then used, along with the relaxation matrices, to derive upper bounds between protons in the coupled spin systems. To account for experimental errors (integration, chemical exchange), 0.2 Å was added to distances derived from the relaxation matrices that were less than 3.0 Å, and 0.3 Å was added to distances greater than 3.0 Å. In addition, a 5.0-Å upper bound was used for drug–DNA contacts determined from 1D NOEs reported previously (Klevit et al., 1986). A summary of the distance constraints is presented in Table IV.

Attempts were made to estimate the uncertainties associated with the distance constraints by simulating the buildup curves of Figure 3a. The simulated curves fit the experimental points reasonably, although there were significant deviations at longer mixing times. Possibilities for the poor fit at long mixing times include spin diffusion or other relaxation processes not modeled in the simulations. Another factor complicating the analysis is the use of a short relaxation delay (2.1 s), combined with different T_1 values for the C11 and adenine C2H protons that resulted in partial saturation and differential scaling of their buildup curves. A NOESY experiment obtained with a recycle delay of 10.2 s and a mixing time of 100 ms revealed that each of the A C2H–H3 NOEs was scaled by a factor of 2.1 relative to the C11 C5H–C6H distance marker. This distortion has been considered in the subsequent analysis.

Figure 3b presents simulated buildup curves for the C11 C5H–C6H and three A C2H–H3 proton pairs along with the experimental points vertically scaled by 2.1 relative to the C11 pair to account for differential saturation. The fit of the simulated and experimental data are good at 50 ms. However, at longer mixing times there are deviations that suggest differential saturation combines with other relaxation phenomena (spin diffusion) to contribute to the behavior of the NOE buildup curves. Taking a conservative approach, the A C2H–H3 distances obtained from the 50-ms NOESY data and those derived from them in the SKEWSY/NOESY analysis were used only as upper bound constraints in the subsequent AMBER calculations. Because of the uncertainties in the data, no attempt was made to either estimate lower bounds or include such terms in the AMBER potential function. The differential saturation phenomena we have observed stress the importance of making T_1 measurements and adjusting recycle delays accordingly when trying to quantify distance information.

Table IV: Calculated Distances and Constraints for the Distamycin A–d(CGCGAATTCGCG)$_2$ Structures

atom pair	structure H_D (Å)	structure W_D (Å)	structure H_I (Å)	deviation H_D vs H_I (Å)	constraint[a] R_0 (Å)
A5 C2H–H3-1	2.2	2.2	2.2	0.0	2.7[b]
A5 C2H–A6 C1′H	4.6	4.7	4.9	0.3	
H3-1–A6 C1′H	2.8	2.8	3.0	0.2	4.2[b]
A6 C2H–H3-2	2.6	2.4	2.6	0.0	2.7[b]
A6 C2H–T7 C1′H	3.2	3.0	3.9	0.7	3.9
A6 C2H–T19 C1′H	3.5	5.0	3.5	0.0	3.5
H3-2–T7 C1′H	2.5	2.5	3.5	1.0	4.0
H3-2–T19 C1′H	4.2	4.8	3.7	−0.5	4.3
A18 C2H–H3-3	2.3	2.3	2.2	−0.1	2.6[b]
A18 C2H–T19 C1′H	3.0	3.2	2.8	−0.2	3.0
A18 C2H–T8 C1′H	3.4	4.0	3.4	0.0	3.4
H3-3–T19 C1′H	2.5	2.8	2.5	0.0	3.3
H3-3–T8 C1′H	2.4	2.7	2.5	0.1	3.8
NH-1–A5 C2H	2.8	2.8	2.7	−0.1	5.0
NH-2–A5 C2H	3.5	3.5	3.7	0.2	5.0
NH-2–A6 C2H	4.0	3.4	3.9	−0.1	5.0
NH-3–A6 C2H	3.5	3.7	3.4	−0.1	5.0
NH-3–A18 C2H	4.4	4.2	3.8	−0.6	5.0
C21HA–A17 C2H	2.3	2.3	2.3	0.0	5.0
C21HB–C9 C1′H	2.6	2.4	3.2	0.6	5.0

[a] Constraint distances are the sum of the upper bound calculated from the relaxation matrix and an additional 0.2 Å if the upper bound was less than 3.0 Å or 0.3 Å if the upper bound was greater than 3.0 Å. [b] Upper bound derived from 50-ms NOESY data. Uncertainty added to only the H3-1–A6 C1′H pair.

AMBER Structures. In the following discussion, we denote the refined uncomplexed DNA structure starting from crystal coordinates (Fratini et al., 1982) as F, the highly constrained complex [K_{NMR} of 10000 (kcal/mol)/Å^2] as H_D, the weakly constrained complex [K_{NMR} of 0.59 (kcal/mol)/Å^2] as W_D, and the highly constrained complex starting from idealized B-form coordinates as H_I. Table IV presents calculated distances for H_D, W_D, and H_I, along with deviations of H_D from H_I, and the NMR constraints. These data show that H_D satisfied all of the constraints. Three distances, those between A6 C2H and T19 C1′H, between A18 C2H and T19 C1′H, and between A18 C2H and T8 C1′H, however, were at their respective constraint values. These proton pairs, along with the H3-2–T19 C1′H pair, violated their respective upper bound constraints when the NMR force constant was reduced. A possible reason will be discussed below. The data also show that H_I satisfied all of the constraints. Three distances, those between A6 C2H and T7 C1′H, between A6 C2H and T19 C1′H, and between A18 C2H and T8 C1′H, were at their respective upper bounds.

The binding energy of distamycin A to d-(CGCGAATTCGCG)$_2$ was 106.3 kcal/mol (H_D) and increased to 129.1 kcal/mol (W_D) upon reduction of K_{NMR}. The difference in binding energy is the sum of bond (−1.2 kcal/mol change between W_D and H_D), angle (−1.4), dihedral (5.0), van der Waals (7.6), electrostatic (14.4), hydrogen bond (0.01), and constraint energies (−1.6). Although several constraints were violated and the binding energy increased, an rms difference between coordinates in H_D and W_D of 0.28 Å indicates

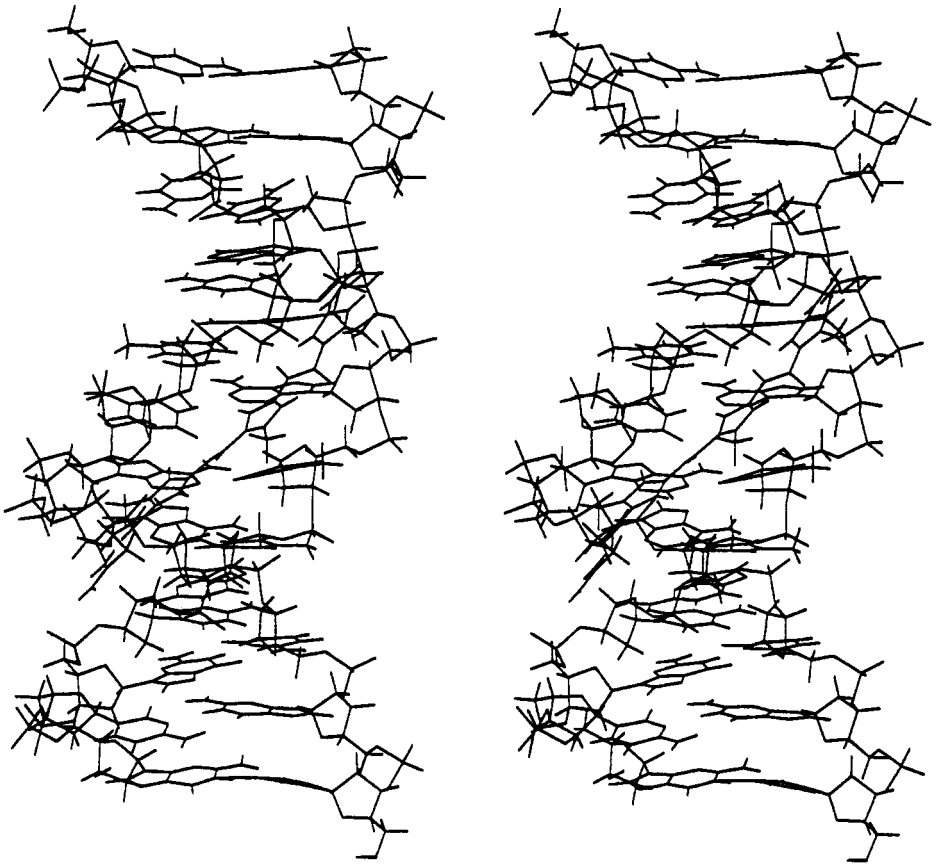

FIGURE 6: Stereo drawing of the distamycin A–d(CGCGAATTCGCG)$_2$ complex. Structure of the drug–DNA complex obtained with an NMR force constant of 10000 (kcal/mol)/Å^2 (structure H_D).

that they are very similar. The difference in total energy of H_D from H_I was +16.6 kcal/mol, and an rms deviation between H_D and H_I including the drug and AATT base pairs was 1.0 Å. The rms deviation between drug molecules alone was 0.6 Å. Further discussion will focus on the general structural characteristics of H_D, W_D, and H_I; differences will be noted where appropriate.

Distamycin A fits snugly into the AATT minor-groove binding site with each of the three pyrrole rings approximately parallel to the walls of the groove (Figure 6). The amidinium group (charge +1) is also positioned in the center of the minor groove at the point of minimum electrostatic potential energy (Lavery et al., 1982). In addition, the data for H_D and W_D in Table IV show that the A5, A6, and A18 C2H protons are in van der Waals contact with the H3-1, H3-2, and H3-3 drug pyrrole protons, respectively, although the A6 C2H–H3-2 distance is somewhat longer than the other two.

If the hydrogen-bond distance (N–N or N–O) is defined as 3.0 Å, only one hydrogen bond, that between A5 N3 and HN1, occurs in this structure. Longer hydrogen bonds exist between HN3 and T20 O2 (3.2 Å), HN5 and T7 O2 (4.0 Å), HN7 and T8 O2 (4.4 Å), HN7 and A18 N3 (3.4 Å), and the drug O1 and G4 amino group (4.3 Å) in structure H_D. Two additional long hydrogen bonds between HN3 and A6 N3 (4.4 Å) and HN5 and T19 O2 (3.6 Å) were observed when the NMR constraints were relaxed (W_D). The hydrogen-bond pattern in H_I is similar to that in H_D, although the HN7–A18 N3 hydrogen bond is 0.4 Å longer in H_I, while the drug O1–G4 amino group and the HN7–T8 O2 hydrogen bonds are 0.5 and 0.6 Å shorter, respectively. The drug–DNA hydrogen-bonding scheme is presented in Figure 7. Note that in H_D HN7 and in W_D HN3 and HN5 are potentially involved in three-center hydrogen bonds with adenine N3 and thymine

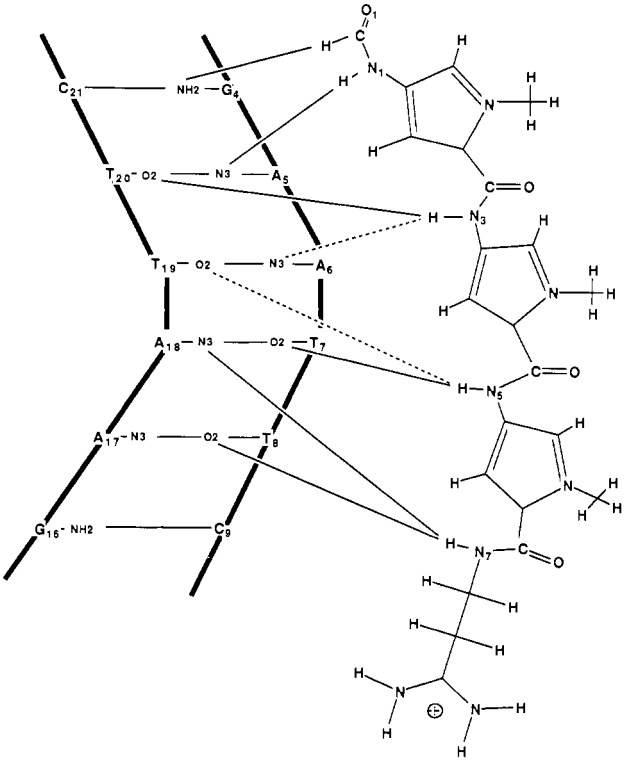

FIGURE 7: Hydrogen-bonding scheme for the distamycin A–DNA complex. Solid lines denote hydrogen bonds in the highly constrained structure (H_D). Dashed lines denote the additional hydrogen bonds that formed when the NMR constraints were relaxed (W_D).

O2 atoms (Jeffrey & Maluszynska, 1982). Longer than normal three-center hydrogen bonds have been reported in

crystal structures of drug–DNA complexes (Kopka et al., 1985c; Pjura et al., 1987; Coll et al., 1987) and will be discussed further below.

The NOESY sequential connectivity patterns and the AMBER calculations suggest that only minor changes in DNA structure occurred due to drug binding. For example, the helical repeat of F, H_D, and W_D were all 9.8 residues/turn, while the helical repeat of H_I was 10.0 base pairs/turn on the basis of local helical twist angles. These data agree with the crystal structure of the dodecamer (Dickerson & Drew, 1981) and also molecular mechanics calculations (Kollman et al., 1982). Although there were local variations, these values are identical with those found in the respective starting structures. rms deviations between H_D and W_D and the initially refined DNA helix (F) were both 0.5 Å. Although changes in DNA structure were small, there are several points worth noting. Van der Waals contacts between A5 C2H and H3-1 and between A6 C2H and H3-2 caused an increase in roll angle (Fratini et al., 1982) (change relative to F of 10° H_D, 6° W_D) at the A5–A6 step. In fact H3-1 is positioned slightly under A5 C2H while H3-2 is positioned slightly above A6 C2H. Thus, the first two pyrrole rings can be seen to wedge themselves against and between these residues. The constraints on T19 C1′H caused a repositioning of T19 closer to A18, which resulted in an increased buckle (defined as the angle between the bases after the propeller twist has been set to zero) of the T19–A6 pair (change relative to F of 4° H_D, 0.5° W_D). Similarly, the constraints on T7 C1′H caused a repositioning of the T7 base closer to A6, which resulted in an increased buckle of T7 and A18 (a change relative to F of 20° H_D, 16° W_D). Finally, the constraints on T8 C1′H caused an increase in the buckle (change relative to F of 14° H_D, 6° W_D) of the T8–A17 pair. In H_I, the T19 base was moved closer to T20 rather than A18, which caused an increase in the buckle of the A6–T19 base pair of 7° relative to H_D, while the buckle of the T7–A18 and T8–A17 base pairs was reduced by 6° and 18°, respectively, relative to H_D.

Inspection of minor-groove widths revealed that the minor groove of the free DNA increased 1.4–2.4 Å relative to the starting structure upon energy refinement (Fratini et al., 1982). It then decreased 0.5–2.0 Å to an average value of 11.2 Å upon refinement of the complex. In the crystal structure of the free DNA, the groove is so narrow at points that it must widen to accommodate the drug. The groove widths of the symmetry-related sequences are quite different from one another in the crystal, so its is difficult to know which to compare with. The minor-groove width of H_I decreased from 11.8 Å for the classical B-form DNA to an average of 11.3 Å. In addition, the minor-groove width of a complex between distamycin A and idealized B-form coordinates refined without NMR constraints decreased to an average value of 11.2 Å.

Further structural analysis revealed that pyrrole rings 1 and 2 are nearly parallel to one another (dihedral angle between rings 1 and 2, −3° H_D, −9° W_D, −1° H_I), while ring 3 is rotated significantly (dihedral angle between rings 2 and 3, 43° H_D, 52° W_D, 36° H_I) to conform to the groove of the helix. In addition, the O1′ atoms that lie along the walls of the minor groove were found to stack within 3.5–4.2 Å over the center of each of the three pyrrole rings. Specifically, the O1′ atoms of pairs A6–C21, T7–T20, and T8–T19 stack over rings 1, 2, and 3, respectively. Reduction of the NMR force constant caused an increase of 0.3 Å in the T8 O1′–pyrrole 3–T19 O1′ distance. The other two distances were not significantly affected. The possible significance of this will be discussed below. This type of stacking interaction has also been seen in crystal structures of nucleosides and nucleotides (Bugg et al., 1971), Z-DNA (Wang et al., 1979), and netropsin with d-$(CGCGAATTCGCG)_2$ (Kopka et al., 1985c).

Discussion

Analysis of spin diffusion in strongly coupled spin systems has been the subject of extensive study (Kalk & Berendsen, 1976; Kumar et al., 1981; Keepers & James, 1984; Olejniczak et al., 1986). We believe that the SKEWSY/NOESY method (Bremer et al., 1984) is excellent for analyzing small groups of strongly coupled spins because only those spins that are involved in spin diffusion within the set need to be included in the analysis. We have shown that other spins which are coupled to only one member of the system can be neglected without error. In contrast, accurate methods of accounting for spin diffusion that employ the measurement of the actual magnetization transferred (as opposed to rates of transfer) must include all spins in the system that interact, not just those involved in spin diffusion among themselves.

One of the problems associated with molecular mechanics calculations is in finding the global energy minimum. Our incorporation of distance constraints into the potential function should reduce this problem while adding experimental data specific to this system into the calculation. An important test of these calculations is to determine whether two different starting structures can be refined to the same final structure. In this regard we have refined complexes from both the crystal coordinates (Fratini et al., 1982) (H_D) and idealized B-form coordinates (Arnott and Chandrasekaran, private communication) (H_I). Structures H_D and H_I are similar in many respects as evidenced by a rms fit of the drug and central AATT region of 1.0 Å, by a rms fit of the drugs alone of 0.6 Å, and by small deviations in the constrained distances as shown in Table IV. The data also show that global structural characteristics such as drug conformation, hydrogen bonding, and van der Waals contacts are similar. There were, however, local structural differences between H_D and H_I. Most notable was the positioning of T19 under A6 in H_D and above A6 in H_I. In addition, although there were local variations, the average helical repeat of each structure was the same as that of the starting structure, indicating that the AMBER potential function does not move the DNA significantly unless many NMR constraints are applied. Finally, the formamide and propylamidinium portions of the drug are oriented slightly differently, giving hydrogen-bond lengths between DNA and drug O1 and HN7 atoms that were slightly different in H_D and H_I. Thus, on the local level, the calculations show that there are small structural perturbations, but they are not defined with very high precision. As new NMR techniques that provide larger numbers of more accurate constraints are developed in conjunction with more accurate molecular mechanics potential functions, our ability to observe finer changes in the solution structure of DNA will improve.

The pyrrole rings in our structure are aligned to an 5′-AAT-3′ sequence with rings 1, 2, and 3 close to A5, A6, and A18 respectively. This binding site is different from that found in the crystal structure of distamycin A with d-$(CGCAAATTTGCG)_2$ (Coll et al., 1987) in which the three pyrrole rings are aligned to a 5′-ATT-3′ sequence, although an 5′-AAT-3′ site is available to the drug. Occupation of different binding sites may in part account for the differences in the dihedral angles of the drug in the two structures [1 and 2; Coll et al. (1987) 15°, H_D 4°; 2 and 3, Coll et al. (1987) 11°, H_D 46°]. It is interesting to note in structures H_D, W_D, and H_I that the A6 C2H–H3-2 distance is somewhat longer than the other two A C2H–H3 pairs, indicating a bowing out

of the drug to better accommodate the helical twist of the DNA.

The NOESY sequential connectivity assignments and the AMBER calculations support the conclusion that only small structural perturbations of the DNA occur upon drug binding. The same conclusion has come from NMR (Patel et al., 1986) and crystallographic studies (Kopka et al., 1985a) of netropsin and from crystallographic studies of Hoechst 33258 (Pjura et al., 1987).

Analysis of H_D and W_D revealed potential three-center hydrogen bonds between drug amide and A N3 and T O2 atoms similar to those of the distamycin A–d-$(CGCAAATTTGCG)_2$ (Coll et al., 1987), the netropsin–d-$(CGCGAATTCGCG)_2$ (Kopka et al., 1985a), and the Hoechst 33258–d$(CGCGAATTCGCG)_2$ (Pjura et al., 1987) crystal structures. As pointed out by Kopka et al. (1985a), these are the same hydrogen bonds that occur in the spine of hydration of the free DNA sequence (Drew & Dickerson, 1981). A characteristic feature of all of these structures is the presence of at least several abnormally long hydrogen bonds between drug and DNA minor-groove atoms. In H_D, W_D, and H_I, most of the hydrogen bonds between amide and A N3 and T O2 atoms are too long to be considered normal (3.0 Å), with four of seven being longer than 3.3 Å. In the crystal structure of distamycin A with d-$(CGCAAATTTGCG)_2$ (Coll et al., 1987) the distances between drug amide N3 and potential hydrogen-bonding sites T7 and T19 O2 were 3.9 and 4.4 Å, respectively. It was suggested that this was due to a different periodicity of the drug pyrrole–amides and the DNA. In fact, five of six hydrogen bonds between drug amide and DNA T O2 and A N3 atoms were greater than 3.0 Å, with two longer than 3.3 Å. In the netropsin complex four of six amide–DNA hydrogen bonds were 3.3 Å or longer (Kopka et al., 1985c), and in the recently reported crystal structure of Hoechst 33258 and $d(CGCGAATTCGCG)_2$ (Pjura et al., 1987), in which the benzimidazole NH groups form three-center hydrogen bonds with A N3 and T O2 atoms, three of four are longer than 3.3 Å. Long hydrogen bonds thus seem to be a common motif for these minor-groove binders. We agree with Kopka et al. (1985c) that the hydrogen-bond energy is mostly electrostatic in character, and in the hydrophobic environment of the minor groove the interactions may not be dissipated with distance as quickly, thus providing stabilization in spite of their length.

Our calculations suggest that the width of the minor groove in the complex is narrowed relative to that of "fiber" B DNA. Energy refinement of the $d(CGCGAATTCGCG)_2$ crystal structure (Fratini et al., 1982) without drug resulted in an expansion of the minor groove. Subsequent refinement with distamycin A reduced it again to an average of 11.2 Å, compared to the idealized B-form minor-groove width of 11.8 Å. We determined, however, that the compaction of the groove is due to the AMBER potential function rather than the NMR constraints since the minor groove was narrowed to the same degree in a complex refined without NMR distance constraints. Narrow minor grooves have been seen in other structures' A-T-rich sequences. For example, the minor groove of distamycin A with $d(CGCAAATTTGCG)_2$ (Coll et al., 1987) was reported to be narrow. Whether the drug occupies an already narrow groove, as seen in the $(A)_6$-containing sequence characterized recently (Nelson et al., 1987), or whether the drug actually widens it will require further analysis. The crystal structure of $d(CGCGAATTCGCG)_2$ (Fratini et al., 1982) and of its complex with netropsin (Kopka et al., 1985c) shows that the drug actually widens the already narrow minor groove from 0.5 to 2.0 Å, with an average value identical with that of structure H_D. A similar expansion is seen in the complex of this sequence with Hoechst 33258 (Pjura et al., 1987).

Our structures and recent work on the distamycin A–d-$(CGCAAATTTGCG)_2$ complex (Coll et al., 1987), the netropsin–$d(CGCGAATTCGCG)_2$ complex (Kopka et al., 1985b), the netropsin–$d(GGAATTCC)_2$ complex (Patel & Shapiro 1985), the Hoechst 33258–$d(CGCGAATTCGCG)_2$ complex (Pjura et al., 1987), and the 1-methyl-4-[4-[[4-[(1-methylpyridinium-4-yl)amino]anilino]carbonyl]anilino]-quinolinium dibromide (SN 6999)–$d(GCATTAATGC)_2$ complex (Leupin et al., 1986) suggest that these minor-groove-binding drugs are in van der Waals contact with the DNA atoms along the minor groove. Specifically, we note that the O1′ atoms stack over the center of each of the three pyrrole rings. Specific van der Waals interactions between netropsin and DNA O1′ atoms have also been noted (Kopka et al., 1985c). This type of interaction, a heteroatom stacking over an aromatic ring, has also been found in crystal structures of nucleosides and nucleotides and has been suggested as a stabilizing force in the binding of aromatic molecules to nucleic acids (Bugg et al., 1971) and also Z-DNA (Wang et al., 1979). It provides an additional explanation for the fact that increasing numbers of *N*-methylpyrrole rings increase the stability of the complex, although hydrophobic effects and hydrogen bonding probably also play a role (Zimmer et al., 1975).

A possible explanation for the distance constraint violations of T8 and T19 (W_D) may be found in the fact that the T8 O1′–pyrrole 3–T19 O1′ distance is 0.3 Å shorter in the highly constrained structure than in the weakly constrained structure. Thus, the NMR data effectively increase the stacking between the T8 and T19 O1′ atoms and pyrrole ring 3. This suggests that the interaction is important but is simply not well modeled by the AMBER potential function, thus causing violations when the constraints were relaxed.

Another possibility is that the drug undergoes small conformational fluctuations within the minor groove during the mixing time. A measured NOE would then be a distance weighted (inverse sixth power) average that would cause a proton–proton distance to appear shorter than the actual "average" distance. Since only 4 of the possible 19 constraints were violated, this possibility seems less likely.

Conclusions

The SKEWSY/NOESY method can be used to accurately determine distances among a set of dipolar-coupled spins. Spins that interact with only one member of the set can be neglected without error. The effect of a neglected spin is to increase the apparent spin–lattice relaxation of the spin to which it is coupled.

The distamycin A–$d(CGCGAATTCGCG)_2$ complex is characterized by van der Waals contacts between adenine C2H and drug H3 protons, potential three-center hydrogen bonds between drug amide and adenine N3 and thymine O2 atoms that protrude from the minor groove, and stacking of DNA O1′ atoms over each of the three pyrrole rings. The first two rings of the drug are approximately parallel, while the third ring is turned to conform to the rotation of the helix. No large structural changes were observed for the DNA.

There have been a number of suggestions for the high stability of distamycin A–DNA complexes. These include electrostatic forces, hydrogen bonding, and hydrophobic effects. The importance of electrostatic forces is still uncertain, but it is certainly not the only factor since 6 M urea and 0.1 M

NaCl do not dissociate the complex (Hahn, 1975). In addition, theoretical calculations suggest that hydrogen-bond formation is not required for the binding of netropsin and presumably also distamycin A to the minor groove (Zakrzewska et al., 1983). We suggest that the dipole-induced dipole interactions of the sugar O1′ atoms and the three *N*-methylpyrrole rings contribute to the stability of the complex and provide a molecular basis for the fact that binding is enhanced by the addition of *N*-methylpyrrole rings.

ACKNOWLEDGMENTS

We kindly acknowledge Professor R. Klevit for providing us with an initial distamycin A–DNA sample and for fruitful collaboration in the initial stages of the project. We also acknowledge Dr. U. C. Singh for providing us with the AMBER FORTRAN code and J. Hubbard and W. Ross for helpful discussions of the usage of the program. Finally, we thank Dr. S. Holbrook for providing programs with which to calculate the various helical parameters.

Registry No. Distamycin A–d(CGCGAATTCGCG), 116324-69-7.

REFERENCES

Berman, H. M., Neidle, S., Zimmer, C., & Thrum, H. (1979) *Biochim. Biophys. Acta 561*, 124.

Bremer, J., Mendz, G. L., & Moore, W. J. (1984) *J. Am. Chem. Soc. 106*, 4691.

Bugg, C. E., Thomas, J. M., Sundaralingam, M., & Rao, S. J. (1971) *Biopolymers 10*, 175.

Caldwell, J., & Kollman, P. (1986) *Biopolymers 25*, 249.

Coll, M., Frederick, C. A., Wang, A. H.-J., & Rich, A. (1987) *Proc. Natl. Acad. Sci. U.S.A. 84*, 8385.

Dervan, P. B. (1986) *Science (Washington D.C.) 232*, 464.

Dewar, M. J. S., & Thiel, W. (1977) *J. Am. Chem. Soc. 99*, 4899.

Dickerson, R. E., & Drew, H. R. (1981) *J. Mol. Biol. 149*, 761.

Drew, H. R., & Dickerson, R. E. (1981) *J. Mol. Biol. 151*, 535.

Drobny, G., Pines, A., Sinton, S., Weitekamp, D., & Wemmer, D. (1979) *Faraday Div. Chem. Soc. Symp. 13*, 49.

Fratini, A. V., Kopka, M. L., Drew, H. R., & Dickerson, R. E. (1982) *J. Biol. Chem. 257*, 14686.

Hahn, F. E. (1975) in *Antibiotics III, Mechanism of Action of Antimicrobial and Antitumor Agents* (Corcoran, J. W., & Hahn, F. E., Eds.) p 79, Springer-Verlag, New York.

Jeener, J., Meier, B. H., Bachmann, P., & Ernst, R. R. (1979) *J. Chem. Phys. 71*, 4546.

Jeffrey, G. A., & Maluszynska, H. (1982) *Int. J. Biol. Macromol. 4*, 173.

Kalk, A., & Berendsen, H. J. C. (1976) *J. Magn. Reson. 24*, 343.

Keepers, J. W., & James, T. L. (1984) *J. Magn. Reson. 57*, 404.

Klevit, R. E., Wemmer, D. E., & Reid, B. R. (1986) *Biochemistry 25*, 3296.

Kollman, P., Keepers, J. W., & Weiner, P. (1982) *Biopolymers 21*, 2345.

Kopka, M. L., Yoon, C., Goodsell, D., Pjura, P., & Dickerson, R. E. (1985a) *Proc. Natl. Acad. Sci. U.S.A. 82*, 1376.

Kopka, M. L., Yoon, C., Goodsell, D., Pjura, P., & Dickerson, R. E. (1985b) *J. Mol. Biol. 183*, 553.

Kopka, M. L., Yoon, C., Goodsell, D., Pjura, P., & Dickerson, R. E. (1985c) in *Structure & Motion: Membranes, Nucleic Acids & Proteins* (Clementi, E., Corongiu, G., Sarma, M. H., & Sarma, R. H., Eds.) p 461, Adenine, Guilderland, NY.

Krey, A. K., Allison, R. G., & Hahn, F. E. (1973) *FEBS Lett. 29*, 58.

Kumar, A., Wagner, G., Ernst, R. R., & Wüthrich, K. (1981) *J. Am. Chem. Soc. 103*, 3654.

Lavery, R., Pullman, A., & Pullman, B. (1982) *Theor. Chim. Acta 62*, 93.

Lavery, R., Zakrzewska, K., & Pullman, B. (1986) *J. Biomol. Struct. Dyn. 3*, 1155.

Leupin, W., Chazin, W. J., Hyberts, S., Denny, W. A., & Wüthrich, K. (1986) *Biochemistry 25*, 5902.

Macura, S., & Ernst, R. R. (1980) *Mol Phys. 41*, 95.

Nelson, H. C. M., Finch, J. T., Bonaventura, L. F., & Klug, A. (1987) *Nature (London) 330*, 221.

Olejniczak, E. T., Gampe, R. T., Jr., & Fesik, S. W. (1986) *J. Magn. Reson. 67*, 28.

Patel, D. J. (1982) *Proc. Natl. Acad. Sci. U.S.A. 79*, 6424.

Patel, D. J., & Shapiro, L. (1985) *Biochimie 67*, 887.

Patel, D. J., & Shapiro, L. (1986) *J. Biol. Chem. 261*, 1230.

Patel, D. J., Shapiro, L., & Hare, D. (1987) *Annu. Rev. Biophys. Biophys. Chem. 16*, 423.

Pjura, P. E., Grzeskowiak, K., & Dickerson, R. E. (1987) *J. Mol. Biol. 197*, 257.

Taylor, J. S., Schultz, P. G., & Dervan, P. B. (1984) *Tetrahedron 40*, 457.

Wang, A., Quigley, G. J., Kolpak, F. S., Crawford, J. L., van Boom, J. H., van der Marel, G., & Rich, A. (1979) *Nature (London) 282*, 680.

Weiner, S. J., Kollman, P. A., Case, D. A., Singh, U. C., Ghio, C., Alagona, G., Profeta, S., & Weiner, P. (1984) *J. Am. Chem. Soc. 106*, 765.

Weiner, S. J., Kollman, P. A., Nguyen, D. T., & Case, D. A. (1986) *J. Comput. Chem. 7*, 230.

Zakrzewska, K., Lavery, R., & Pullman, B. (1983) *Nucleic Acids Res. 11*, 8825.

Zakrzewska, K., Lavery, R., & Pullman, B. (1987) *J. Biomol. Struct. Dyn. 4*, 833.

Zimmer, C. (1975) *Prog. Nucleic Acid Res. Mol. Biol. 15*, 285.

Zimmer, C., Luck, G., Thrum, H., & Pitra, C. (1972) *Eur. J. Biochem. 26*, 81.